Supporting Information

Linton et al. 10.1073/pnas.1002471107

SI Text

Detailed Descriptions of the Methods. ***Reagents and antibodies.*** 1 fluoro 2,4 dinitrobenzene (FDNB) was from Sigma-Aldrich. Antibodies for immunblotting were anti-rhodopsin: 4D2 (1) 1/10,000; anti-CK-B: N-20 (Santa Cruz Biotechnology, Inc.) 1/500; anti-CK-B: 21E10, mouse monoclonal, 1/1,000 (2); anti-uMtCK: C-18 (Santa Cruz) 1/500; anti-synaptotagmin: P65 (gift from S. Bajallieh, University of Washington, Seattle) 1/5,000; anti-cytochrome oxidase 1: COX-1 (Mitosciences) 1/2,000.

Animals. WT, CK-B-/- (3), and CK–/– dko mice (4) were generated and genotyped as reported. The adult mice (2–5 months old) were housed in a central animal facility at 21 °C (12 h:12 h light:dark cycle) and used for immunocytochemistry, biochemical, and electroretinogram (ERG) analyses. Zebrafish (AB/WK) were maintained as an inbred stock in the University of Washington Zebrafish Facility. Adult fish and larvae were maintained at 28.5 °C in reverse-osmosis distilled water reconstituted with salts and vitamins on a 10/14 h dark/light cycle. All animal procedures were approved by each of the local Institutional Animal Care and Use Committees.

Cell Biology. ***Immunocytochemistry.*** For immunocytochemistry eyes from WT and CK-B-/- mice were dissected, immersion-fixed in cold 4% paraformaldehyde for 1 h, and cryoprotected in 10–25% graded sucrose solutions, and 8-μm vertical retinal cryosections were cut. For immunostaining, retinal sections were incubated in 50 mM Tris, 0.5 M NaCl (pH 8.6) containing 1% BSA and 0.5% Triton-X (TBST), followed by incubation with primary antibody to CK-B (21E10 1:1,000) (2) and secondary antibody conjugated to Alexa 568 (red color). DAPI was used for nuclear staining. For double-label immunostaining experiments against CK-B and synaptotagmin, retinal sections from WT and CK-B$^{-/-}$ mice were incubated in PBS (pH 7.4) containing 5% goat serum, 1 mg/mL BSA, and 0.3% Triton-X, followed by incubation with primary antibodies to CK-B (21E10, mouse monoclonal, 1:1,000) (2) and to synaptotagmin (p65, rabbit polyclonal, 1:1,000; gift from Sandy Bajjalieh, Seattle, WA). Secondary antibodies were coupled to Alexa 568 and 633 (Molecular Probes). Sytox-green (Molecular Probes) was used as nuclear stain. All secondary antibodies and nuclear stains were used according to the manufacturer's recommendations.

Serial sectioning/immunoblot analyses. Adult Long Evans rats were either dark-adapted O/N or exposed to ambient illumination for several hours. Rats were killed and eyes harvested and dissected in DMEM/F12 media (Invitrogen). Retina dissection and serial sectioning were as described (5). During dissection and flat-mounting, dark-adapted retinas were visualized with dim red light and night-vision goggles. Following freezing, retina fragments were exposed to ambient light and serially sectioned at 10 μM. Each section was dissolved in 50 μL of Buffer M, 1% n-octyl β-D-glucopyranoside, and stored at −20 °C. SDS gel electrophoresis was performed on 5 μL of each section. Salamander retinas were sectioned by a similar method except that they were flattened and frozen by using a polished metal surface at dry ice temperature forced on top of the retina by using a drill press. Solubilized proteins were separated by SDS PAGE, transferred, and probed with primary. Antibody 4D2 was used for both mouse and salamander rhodopsin. The blots were probed with secondary and quantified on an Odyssey Infrared Imaging System (LI-COR Biosciences). Datasets for rat retinas were averaged by aligning peak sections for rhodopsin, synaptotagmin, and uMtCK. A simple algebraic alignment was used to correct for variations in tissue thickness.

Biochemistry. ***Creatine kinase assays.*** Two mouse retinas were dissected in room light and homogenized (Teflon/glass dounce) in 0.5 ml of "Buffer M": (in mM) 225 mannitol, 75 sucrose, 1 EGTA, and 5 Hepes (pH 7.0). Serial sections were analyzed by solubilizing the section in the same buffer including 1% n-octyl β-D-glucopyranoside. Approximately 10% of the solubilized section was used per assay. CK activity was measured by adding 10 mM PCr to a mix of retina homogenate, 10 mM ADP, 5 mM glucose, hexokinase, glucose-6-phosphate dehydrogenase, and 10 mM NADP+ in 50 mM Hepes (pH 7.0). CK activity was monitored by the increase in 340-nm absorbance from NADPH formation (6). Neither hexokinase nor glucose-6-phosphate dehydrogenase were affected by FDNB over the range of concentrations used in this study. CK activity in serial sections was measured from 5 μL of section homogenate.

Cytochrome oxidase assays. Cytochrome oxidase activity was measured by monitoring the decrease in absorbance (A_{550}-A_{540}) from reduced cytochrome c added to solubilized serial sections from salamander retina.

DNA assays. DNA was measured by quantifying fluorescence (Ex, 290 nm; Em, 620 nm) from ethidium bromide added to solubilized serial sections from salamander retina.

Rhodopsin phosphorylation. Light-sensitive steps were performed under infrared illumination with night-vision goggles. Mice were dark-adapted overnight, anesthetized by isoflurane, and killed by cervical dislocation, and eyes were removed, dissected, and incubated in an oxygenated solution (in mM) (105 NaCl, 3.6 KCl, 2.4 $MgCl_2$, 1.2 $CaCl_2$, 25 $NaHCO_3$, 5 glucose) at 37 °C for 5 min with or without (w/o) 10 μM FDNB. Then they were either kept in darkness for 30 sec or exposed for 30 sec to intense white light (1 mW/cm^2). Retinas were then homogenized, centrifuged, and proteolyzed (AspN) to release rhodopsin C termini. C-terminal peptides were analyzed by a mass spectrometry method (7).

Electrophysiology. ***Photoreceptor responses and dark current measurements.*** Light-evoked currents from mouse and salamander rod photoreceptors were measured with suction electrodes from finely chopped pieces of retinal tissue as described (8). Clusters of cells with outer segments (OSs) protruding were targeted, and individual rod OSs were drawn gently into a suction electrode containing Ames' media buffered with 10 mM Hepes to pH 7.4. Light-evoked currents were measured following 10-ms flashes from an LED (λ_{max} ~ 470 nm, FWHM ~30 nm) or 30-ms flashes from a tungsten-halogen source passed through an interference filter (λ_{max} ~ 500 nm, FWHM ~15 nm), low-pass filtered at 20 Hz with an 8-pole Bessel filter, and digitized at 1 kHz.

Paired whole cell recordings. Paired pre- and postsynaptic recordings from rods or cones with horizontal or off bipolar cells were obtained by using retinal slices from the aquatic tiger salamander as described elsewhere (9).

Salamanders were decapitated, the cranium hemisected, and the spinal cord pithed. After enucleation, the eye anterior segment

with lens was removed. The resulting eyecup was cut into thirds and a section placed vitreal side down on filter paper (2 × 5 mm, type AAWP, 0.8-μm pores; Millipore). After the retina adhered to the paper, the retina was isolated under chilled amphibian superfusate. The retina and filter paper were cut into 125-μm slices by using a razor blade (#121-6; Ted Pella Inc.) tissue chopper (Stoelting). Retinal slices were rotated 90° to permit viewing of retinal layers when placed under a water immersion objective [40×, 0.7 numerical aperture (NA) or 60×, 1.0 NA] and viewed on an upright fixed stage microscope (Olympus BHWI or Nikon E600FN).

Solutions were applied by a single-pass, gravity-feed perfusion system (~1 mL/min). The normal amphibian superfusate contained (in mM): 111 NaCl, 2.5 KCl, 2 $CaCl_2$, 0.5 $MgCl_2$, 10 Hepes, 5 glucose (pH 7.8). Use of Hepes limited effects of proton feedback (10–12). Solutions were bubbled continuously with 100% O_2.

Patch pipettes were pulled on a PP-830 vertical puller (Narishige USA) from borosilicate glass pipettes (1.2 mm o.d., 0.9 mm i.d., with internal filament; World Precision Instruments) and had tips of ~1 μm o.d. with resistance values of 10–15 MΩ. Horizontal or off bipolar cell pipettes were filled with a solution containing (in mM): 48 CsGluconate, 42 CsCl, 9.4 TEACl, 1.9 $MgCl_2$, 9.4 MgATP, 0.5 GTP, 5 EGTA, 32.9 Hepes (pH 7.2). For photoreceptors, we used a pipette solution containing (in mM): 40 CsGlutamate, 50 CsGluconate, 9.4 TeaCl, 3.5 NaCl, 1 $CaCl_2$, 1 $MgCl_2$, 9.4 MgATP, 0.5 GTP, 5 EGTA, 10 Hepes (pH 7.2). Glutamate helps stabilize recordings and prevent rundown (13).

Cells were voltage clamped by using either a Multiclamp patch-clamp amplifier (Molecular Devices) or Axopatch 200B (Molecular Devices) and Optopatch (Cairn Instruments) amplifiers. Recording pipettes were positioned with Huxley/Wall-style micromanipulators (Sutter Instruments). Currents were acquired by using a Digidata 1322 interface and pClamp 9.2 software (Molecular Devices). Acceptable access resistances for voltage clamp recordings were <50 MΩ. Photoreceptors were voltage clamped at a steady potential of −70 mV and horizontal cells at −50 or −60 mV. We stimulated the photoreceptor with test steps to −10 mV to maximally stimulate Ca^{2+} currents (I_{Ca}) and thereby evoke large and reproducible excitatory postsynaptic currents (EPSCs).

Rods and cones were identified by morphology. Horizontal and off bipolar cells were identified by morphology, response characteristics (14), and appearance after staining with Lucifer yellow (2 mg/mL) or AlexaFluor 568 (Molecular Probes; 0.2 mg/mL).

Electroretinography.

Mouse.

ERGs were performed (15) by using a Ganzfeld bowl, direct current amplifier, and PC-based control and recording unit (Multiliner Vision; VIASYS Healthcare GmbH). Mice were dark-adapted overnight and anesthetized with ketamine (67 mg/kg body weight) and xylazine (12 mg/kg body weight). Pupils were dilated with tropicamide. Single-flash ERG responses were obtained under dark-adapted (scotopic) and light-adapted (photopic) conditions. Light adaptation was accomplished with background illumination of 30 cd^*s/m^2 starting 10 min before recording. Single white-flash stimuli ranged from −4 to 1.5 log cd^*s/m^2 under scotopic and from −2 to 1.5 log cd^*s/m^2 under photopic conditions, divided into 10 and 8 steps, respectively. Ten responses were averaged with an interstimulus interval of either 5 s (for −4 to −0.5 log cd^*s/m^2) or 17 s (for 0 to 1.5 log cd^*s/m^2).

Zebrafish.

ERGs were recorded from eyes isolated from six day postfertilization (dpf) zebrafish larvae as described by Wong et al. (16). A fine tungsten wire loop was used to excise eyes after incubating larvae 5 min in Ringer's solution (in mM) (130 NaCl, 2.5 KCl, 20 $NaHCO_3$, 0.7 $CaCl_2$, 1.0 $MgCl_2$, and 20 glucose) with or without 20 μM FDNB. The solution was bubbled with 95% O_2 and 5% CO_2. Larvae were either dark-adapted 5 min or kept under intense illumination during the incubation with FDNB. ERGs were recorded from isolated eyes by using a glass electrode pushed onto the cornea. Data were acquired and processed as described previously (17). The eyes either were kept in darkness and exposed to 1-sec steps of white light (1 mW/cm^2) or were kept illuminated (1 mW/cm^2) and exposed to 3-sec steps of darkness.

1. Laird DW, Molday RS (1988) Evidence against the role of rhodopsin in rod outer segment binding to RPE cells. *Invest Opthal Vis Sci* 29(3):419–428.
2. Sistermans EA, et al. (1995) Tissue- and cell-specific distribution of creatine kinase B: A new and highly specific monoclonal antibody for use in immunohistochemistry. *Cell Tissue Res* 280(2):435–446.
3. Jost CR, et al. (2002) Creatine kinase B-driven energy transfer in the brain is important for habituation and spatial learning behaviour, mossy fibre field size and determination of seizure susceptibility. *Eur J Neurosci* 15(10):1692–1706.
4. Streijger F, et al. (2005) Structural and behavioural consequences of double deficiency for creatine kinases BCK and UbCKmit. *Behav Brain Res* 157(2):219–234.
5. Song H, Sokolov M (2009) Analysis of protein expression and compartmentalization in retinal neurons using serial tangential sectioning of the retina. *J Proteome Res* 8(1):346–351.
6. Bishop C, Chu TM, Shihabi ZK (1971) Single stable reagent for creatine kinase assay. *Clin Chem* 17(6):548–550.
7. Lee KA, Craven KB, Niemi GA, Hurley JB (2002) Mass spectrometric analysis of the kinetics of in vivo rhodopsin phosphorylation. *Protein Sci* 11(4):862–874.
8. Sampath AP, et al. (2005) Recoverin improves rod-mediated vision by enhancing signal transmission in the mouse retina. *Neuron* 46(3):413–420.
9. Cadetti L, Tranchina D, Thoreson WB (2005) A comparison of release kinetics and glutamate receptor properties in shaping rod-cone differences in EPSC kinetics in the salamander retina. *J Physiol* 569(Pt 3):773–788.
10. DeVries SH (2001) Exocytosed protons feedback to suppress the Ca2+ current in mammalian cone photoreceptors. *Neuron* 32(6):1107–1117.
11. Hirasawa H, Kaneko A (2003) pH changes in the invaginating synaptic cleft mediate feedback from horizontal cells to cone photoreceptors by modulating Ca2+ channels. *J Gen Physiol* 122(6):657–671.
12. Hosoi N, Arai I, Tachibana M (2005) Group III metabotropic glutamate receptors and exocytosed protons inhibit L-type calcium currents in cones but not in rods. *J Neurosci* 25(16):4062–4072.
13. Ishikawa T, Sahara Y, Takahashi T (2002) A single packet of transmitter does not saturate postsynaptic glutamate receptors. *Neuron* 34(4):613–621.
14. Thoreson WB, Nitzan R, Miller RF (1997) Reducing extracellular Cl- suppresses dihydropyridine-sensitive Ca2+ currents and synaptic transmission in amphibian photoreceptors. *J Neurophysiol* 77(4):2175–2190.
15. Seeliger MW, et al. (2001) New views on RPE65 deficiency: The rod system is the source of vision in a mouse model of Leber congenital amaurosis. *Nat Genet* 29(1):70–74.
16. Wong KY, Gray J, Hayward CJ, Adolph AR, Dowling JE (2004) Glutamatergic mechanisms in the outer retina of larval zebrafish: Analysis of electroretinogram b- and d-waves using a novel preparation. *Zebrafish* 1(2):121–131.
17. Van Epps HA, Yim CM, Hurley JB, Brockerhoff SE (2001) Investigations of photoreceptor synaptic transmission and light adaptation in the zebrafish visual mutant nrc. g) *Invest Ophth Vis Sci* 42(3):868–874.
18. Trudeau MC, Zagotta WN (2002) An intersubunit interaction regulates trafficking of rod cyclic nucleotide-gated channels and is disrupted in an inherited form of blindness. *Neuron* 34(2):197–207.
19. Hamill OP, Marty A, Neher E, Sakmann B, Sigworth FJ (1981) Improved patch-clamp techniques for high-resolution current recording from cells and cell-free membrane patches. *Pflugers Arch* 391(2):85–100.
20. Kremmer T, Boldizsar M, Holczinger L (1987) Comparison of high-performance ion-exchange and ion-pair liquid chromatographic methods for the separation of tumour cell nucleotides. *J Chromatogr* 415(1):53–63.
21. Taylor MR, Hurley JB, Van Epps HA, Brockerhoff SE (2004) A zebrafish model for pyruvate dehydrogenase deficiency: Rescue of neurological dysfunction and embryonic lethality using a ketogenic diet. *Proc Natl Acad Sci USA* 101(13):4584–4589.
22. Sweet IR, et al. (2004) Regulation of ATP/ADP in pancreatic islets. *Diabetes* 53(2):401–409.
23. Sweet IR, et al. (2002) Dynamic perifusion to maintain and assess isolated pancreatic islets. *Diabetes Technol Ther* 4(1):67–76.
24. Sweet IR, et al. (2002) Continuous measurement of oxygen consumption by pancreatic islets. *Diabetes Technol Ther* 4(5):661–672.
25. Sweet IR, Gilbert M (2006) Contribution of calcium influx in mediating glucose-stimulated oxygen consumption in pancreatic islets. *Diabetes* 55(12):3509–3519.

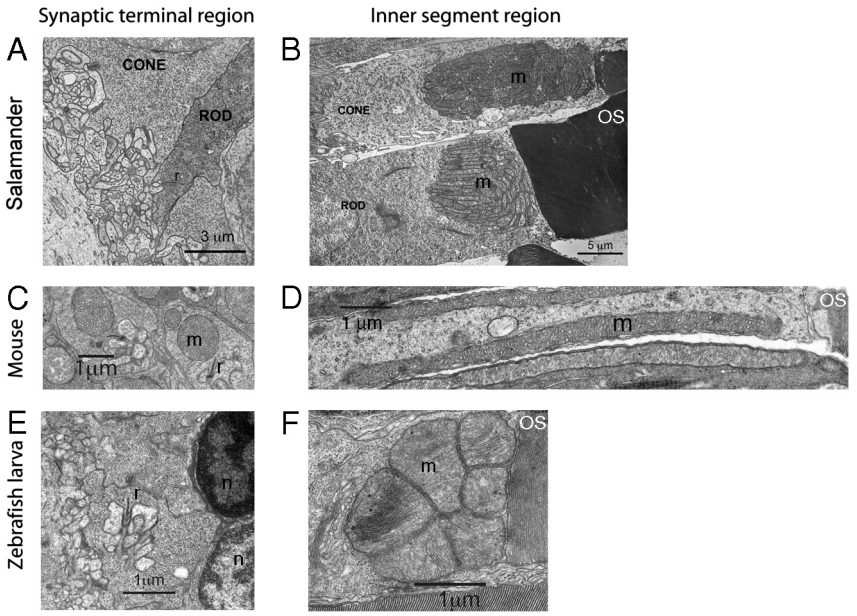

Fig. S1. Comparison by electron microscopy of the synaptic and ellipsoid regions of retinas from the species used in this paper: tiger salamander (avascular), mouse (vascular), and larval zebrafish (avascular). (*A*) Photoreceptor synaptic layer of tiger salamander retina showing a ribbon (*r*) and illustrating the absence of mitochondria in the terminal. (*B*) Ellipsoid region of a salamander rod showing how mitochondria (*m*) are clustered tightly at the base of the OS. (*C*) Photoreceptor synaptic region of mouse retina showing a ribbon (*r*) and mitochondria (*m*). (*D*) Ellipsoid region of mouse rod showing elongated mitochondria that extend from the base of the outer segment towards the nuclear region. (*E*) Photoreceptor synaptic layer of a 5 dpf larval zebrafish retina showing a ribbon (*r*) and illustrating the absence of mitochondria in the terminal. (*F*) Ellipsoid region of a 5 dpf larval zebrafish cone showing how mitochondria (*m*) are clustered tightly at the base of the OS.

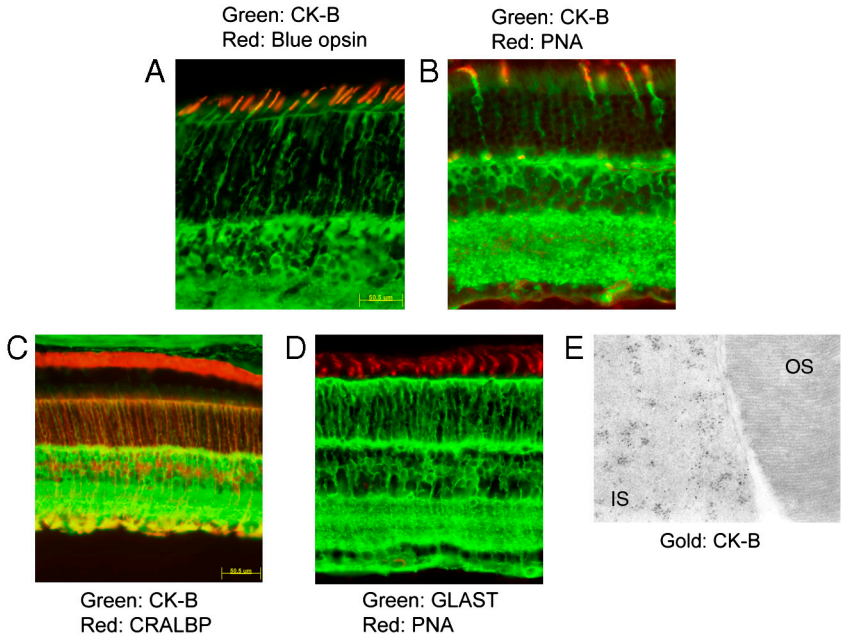

Fig. S2. CK-B is in cones and Müller cells of WT mice. Retinas from WT mice were analyzed by double-label immunofluorescence and immunoelectron microscopy. (*A*) Double labeling for CK-B (*Green*) and blue opsin (*Red*). The CK-B protein is visible in all retinal layers, with high expression in the outer plexiform (synapse) layer. CK-B is present throughout the entire photoreceptor layer including cone inner segments (*Green with Red Cap*) and rods (*Green Protrusions*). There is no colocalization of cone opsin and CK-B in cone outer segments. (*B*) CK-B (*Green*) immunostaining of the entire photoreceptor cell and peanut agglutinin (PNA) (red) staining of the cone matrix sheath confirms the presence of CK-B in the cones. CK-B positive (*Green*) protrusions confirm CK-B expression in rod inner segments. (*C*) Double labeling for CK-B (*Green*) and the Müller cell marker cellular retinaldehyde binding protein (*Red*) shows that CK-B is in the entire Müller cell from the inner to the outer limiting membrane. (*D*) Immunostaining for excitatory amino acid transporter-1 (*Green*) confirms that Müller cells extend from the inner to the outer limiting membrane. PNA (red) staining of the cone matrix sheath shows cones above the outer limiting membrane. (*E*) Immunoelectron microscopy confirms that CK-B is in the inner segment but not in the outer segment of rabbit photoreceptor cells (2). This is a high magnification (60,000×) view of a lower magnification image originally shown by Sistermans et al. (2).

Methods: For immunofluorescence, eyes were dissected, fixed in cold 4% paraformaldehyde for 1 h, and cryoprotected in 10–25% graded sucrose solutions, and 8-μm vertical retinal sections were cut. Sections were preincubated with 2% normal goat serum in TBST (Tris buffered 0.5 M NaCl with 1% BSA and 0.5% Triton X-100) for 1 h at room temperature. The primary antibodies were CK-B (21E10, 1:1,000) (2), blue opsin (SE2107 blue cone visual pigment, 1:500), cellular retinaldehyde binding protein (1:2,000), or excitatory amino acid transporter-1 (1:2,000). Incubation with secondary antibody conjugated to Alexa 488 (green color) was for 2 h. After another wash with TBST, some sections were incubated for 1 h with PNA-rhodamine (red color) diluted 1:400 (Vector Laboratories) in TBST. For double labeling, sections were first incubated with the primary and secondary antibodies for one marker (green color; Alexa 488). They then were incubated with the primary and secondary antibodies to the other marker, by using an additional secondary antibody conjugated to Alexa 568 (red color). Sections were counterstained with the nucleic acid stain DAPI and mounted in Prolong Gold antifade. For immunoperoxidase, eyes from WT mice were dissected and fixed overnight in 4% neutral buffered formalin. After dehydration they were embedded in paraffin and 6-μm sections were picked up on superfrost slides. After deparaffination in xylol and rehydration, sections were treated with 0.5% pepsin in 0.01N HCl for 15 min at 37 °C and rinsed in water for 20 min followed by PBS for 5 min. Endogenous peroxidase activity was blocked by treatment in 3% hydrogen peroxidase in PBS for 20 min followed by a 5 min wash in PBS. After preincubation with 1% normal swine serum in PBS for 30 min, the sections were incubated with primary antibody to CK-B (21E10, 1:2,500) for 3 h at room temperature. Upon extensive rinsing in PBS, they were incubated with secondary antibody conjugated to horseradish peroxidase for 30 min. Following washing in PBS, peroxidase activity was detected with 0.1% 3-amino-9-ethylcarbaxole and 0.03% H_2O_2 in 0.2 M NaOAc (pH 4,9) for 5 min. Sections were counterstained with hematoxylin and mounted in glycerin gelatine.

For immunoelectron microscopy, rabbit eyes were briefly rinsed in physiological saline and fixed immediately by immersion for 2 h in a mixture of 2% paraformaldehyde and 0.1% glutaraldehyde in 0.1 M phosphate buffer (PB), and were stored at 4 °C in 1% paraformaldehyde in PB. Small tissue pieces were immersed in 2.3 M sucrose and directly frozen in liquid nitrogen. Ultrathin sections were cut with glass knives at −100 °C with a Reichert Ultracut S, picked up on Formvar-coated copper grids and transferred onto melting gelatin. Sections were then rinsed 3 times in 0.1 M PB containing 0.1% BSA/0.1% gelatin/0.15% glycerin and incubated with the primary antibody to CK-B (21E10; 1:20,000), followed by a secondary IgG antibody (25 μg IgG/mL). Sections were rinsed and incubated in a protein A-gold solution (10 nM particles). Contrast staining consisted of 0.3% uranyl acetate in a 2% methylcellulose solution. After removal of excess methylcellulose, the grids were dried. The ultrathin sections were examined with a Jeol 1010 transmission electron microscope.

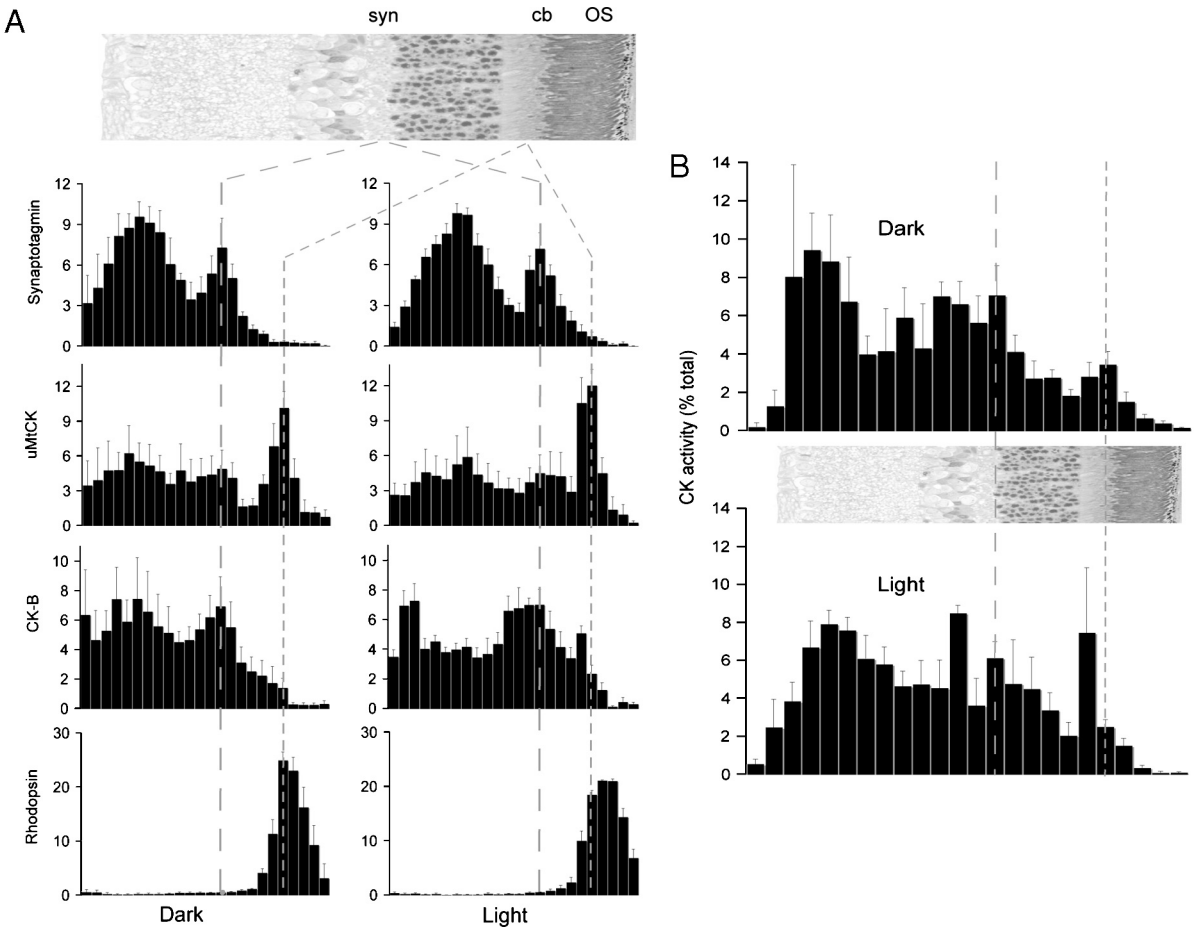

Fig. S3. Distributions of CK in rodent retina in darkness and in light. (*A*) Immunoblots of serial sections of rat retina probed with antibodies to synaptotagmin, uMtCK, CK-B, and rhodopsin. Synaptotagmin marks the locations of synapses in the retina, and rhodopsin marks the location of OSs. The ordinate shows the percentage of the total amount of each protein in the retina that is in each section. The distributions represent the averages and standard error of the mean for five sets of sections for dark and four for light. (*B*) Percent total CK activity in serial sections of rat retinas averaged from four section sets in dark and four in light.

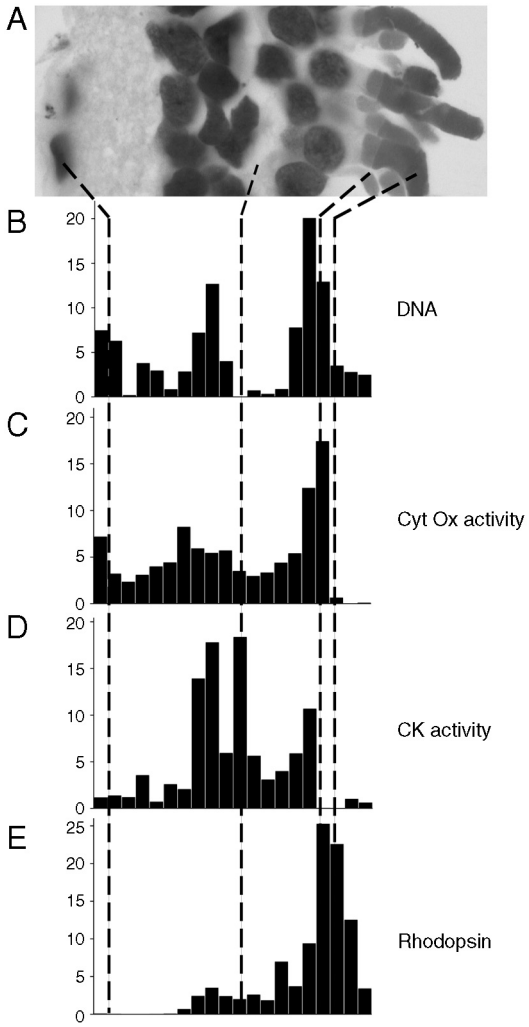

Fig. S4. Distribution of CK activity in salamander retina. (*A*) Confocal micrograph of a section of salamander retina showing the locations of the nuclear and outer segment layers. The remaining panels show analyses of 5-μm serial sections of salamander retina assayed for (*B*) DNA, (*C*) cytochrome oxidase activity, (*D*) creatine kinase activity, and (*E*) rhodopsin immunoreactivity. The ordinate reports the percent in each section of the total activity in the retina. The result from the set of serial sections with highest resolution is shown. Distributions that were qualitatively similar, but lower resolution, were found with two additional sets of serial sections. Enzymatic activities were measured in duplicate.

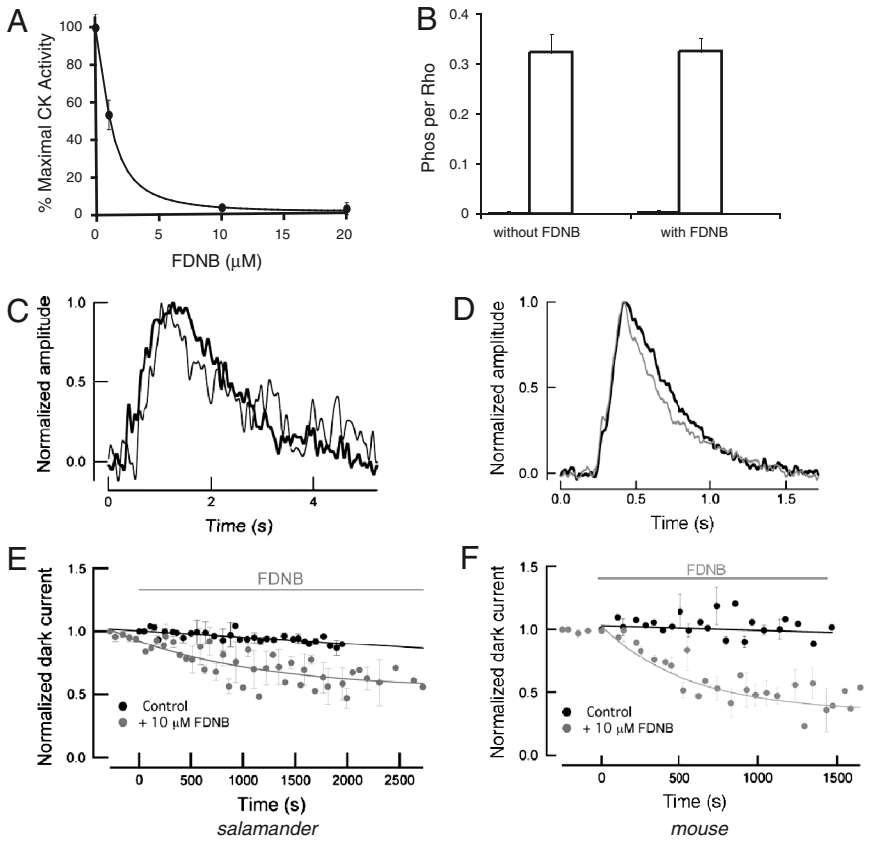

Fig. S5. Effects of FDNB on CK and energy-dependent activities. (*A*) CK activity from 0.5% of a mouse retina homogenate was evaluated over a range of concentrations of FDNB. (*B*) 10 μM FDNB does not affect light-stimulated phosphorylation of rhodopsin in intact mouse retinas. (*C*) Dim flash responses from salamander rods in the presence (*Thin Gray Line*) or absence (*Thick Black Line*) of 10 μM FDNB. (*D*) Dim flash responses from mouse rods in the presence (*Thin Gray Line*) or absence (*Thick Black Line*) of 10 μM FDNB. (*E*) Measurements of peak dark current in salamander rods during saturating flashes plotted vs. duration of recording. Dark currents were normalized to their maximum. (*F*) Measurements of peak dark current in mouse rods during saturating flashes plotted vs. duration of recording. Dark currents were normalized to their maximum. The decline in peak dark current with FDNB (*Gray Bar*) was fit to an exponential function with $\tau = 560$ sec.

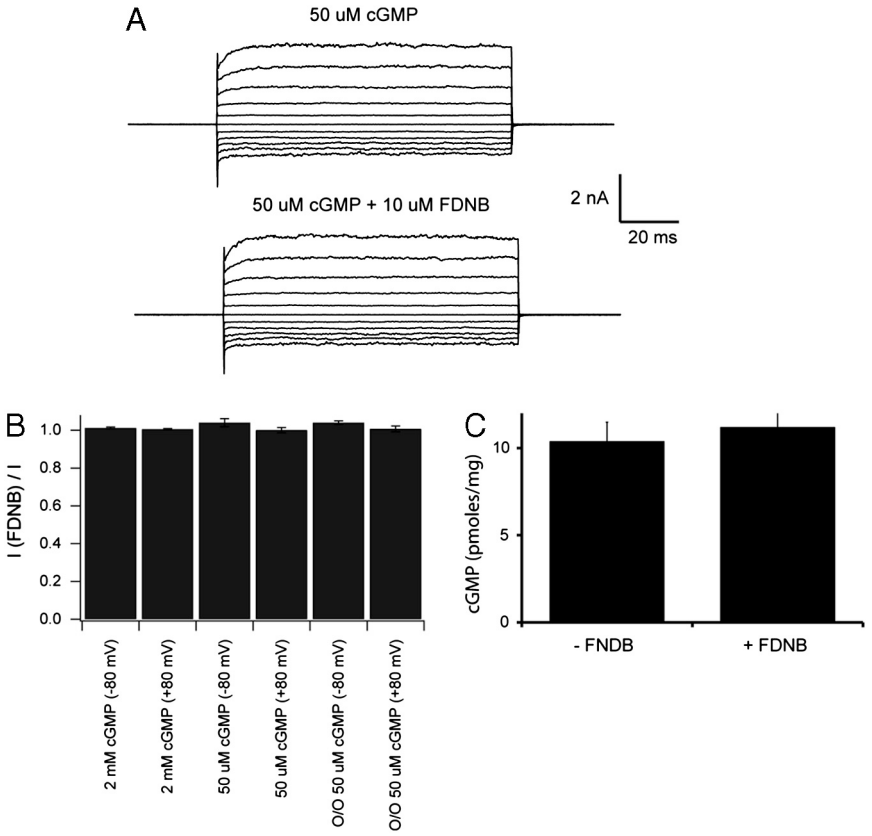

Fig. S6. FDNB (10 μM) does not affect cGMP-gated channel activity or cGMP levels. Bovine CNGA1/CNGB1 heteromeric channels were expressed in Xenopus oocytes as previously described (18). Patch-clamp recordings were made in both the inside-out and outside-out configurations (19). Both the pipet and the bath solutions contained the following (in mM): 130 NaCl, 0.2 EDTA, 3 Hepes (pH 7.2). For inside-out patches the bath solution was supplemented with cGMP and 10 μM FDNB as indicated. For outside-out patches, 50 μM cGMP (about a half-saturating concentration) was added to the pipet solution and 10 μM FDNB was added to the bath solution as indicated. The current was recorded with voltage steps from 0 mV to between −100 and +100 mV in 20-mV increments, and the current in the absence of cGMP was subtracted (for inside-out patches). (*A*) Currents recorded in an inside-out patch with 50 μM cGMP in the absence (*Top*) and presence (*Bottom*) of 10 μM FDNB. (*B*) The fraction of channel current remaining with 10 μM FDNB [I(FDNB)/I] under the following conditions: internal or external FDNB, 2 mM or 50 μM cGMP, and −80 or +80 mV. There was no detectable effect of 10 μM FDNB under any of these conditions. (*C*) Incubating mouse retinas with FDNB does not affect the cGMP content of the retina. C57BL mice were dark-adapted overnight. The dissections and all tissue treatments were carried out under infrared light by using night-vision goggles. Mice were killed by cervical dislocation. The eyes were removed and hemisected with small scissors. Retinas were dissected from the eyecups and were placed in petri dishes with an oxygenated physiological solution (105 mM NaCl, 3.6 mM KCl, 2.4 mM $MgCl_2$, 1.2 mM $CaCl_2$, 25 mM $NaHCO_3$, 5 mM glucose) for 15 min. At the end of each experiment, retinas were placed into 1.5-mL tubes with 300 μL of 100% DMSO and subsequently homogenized. The tubes were then snap-frozen in liquid nitrogen, lyophilized, and resuspended in 200 μL water. A 20-μL aliquot was used to determine protein content (BioRad DC assay). The remaining sample was centrifuged at 14,000 × *g* for 10 min, and the supernatant was removed and kept at −80 °C. cGMP levels were determined by using the Amersham cGMP Enzymeimmunoassay Biotrak System.

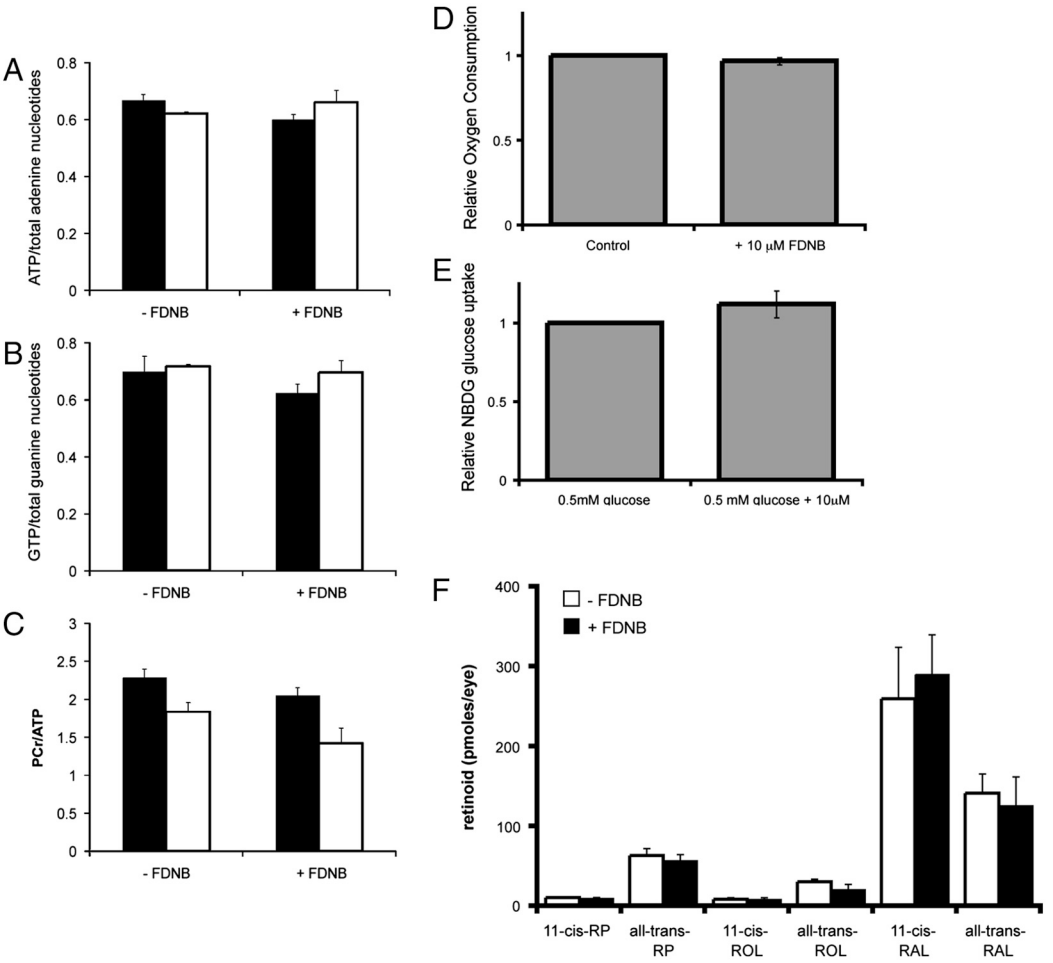

Fig. S7. FDNB (10 μM) does not affect dark-adapted (*Black Bars*) or light-adapted (*White Bars*) ratios of ATP/(total adenine nucleotides) (*A*) and GTP/(total guanine nucleotides) (*B*), and it slightly reduces the PCr/ATP ratio (*C*). C57BL mice were either dark-adapted overnight or exposed to ambient illumination for >2 h. Nucleotides were extracted as described for the cGMP measurements in Fig. S3. Nucleotides were separated by injecting 50 μL of retinal extract onto a Partisphere SAX (4.6 mm × 125 mm; Whatman) ion exchange HPLC column. Elution was carried out with a mobile phase containing water ("A") and 0.5 M $(NH_3)HPO_4$ pH 7.0 ("B"). The program was as follows 99% A/ 1% B at time 0 to 85% A/ 15% B at 10 min, 50% A/ 50% B at 20 min, 30% A/ 70% B at 30 min, and 20% A/ 80 % B at 33.75 min. Detection and quantification were carried out by measuring absorption at 256 nm for nucleotides and at 210 nm for PCr by using a dual channel detector (20, 21). (*D*) 10 μM FDNB does not affect O_2 consumption by mouse retinas. A flow culture system was used to measure O_2 consumption rate as described previously (22–24). Mouse retinal pieces cut from four retinas were loaded into each chamber as described previously for pancreatic islets except that no Cytodex beads were added. O_2 tension was measured by detecting the phosphorescence lifetime (Tau Theta, Inc.) of an O_2-sensitive dye (platinum tetrapentafluorophenyl porphyrin) painted on the inside of the tubing several centimeters upstream and downstream of the perifusion chamber (25). The O_2 consumption rate was calculated as the flow rate (approximately 65 μL/ min) times the difference between inflow and outflow levels of O_2. (*E*) 10 μM FDNB does not affect glucose uptake by retinas from adult zebrafish. Eyes were obtained from the transgenic zebrafish line *Tg(TαC:tdTomato)* that expresses tdTomato in cone photoreceptors under the cone α transducin promoter. For loading experiments with 2-[*N*-(7-nitrobenz-2-oxa-1,3-diazol-4-yl)amino]-2-deoxyglucose (2-NBDG), both retinas from the same fish were used for loading in the presence of FDNB and in the absence as a control. Fish were dark-adapted overnight, and retinas were dissected without the retinal pigment epithelium. Dissections and experiments were performed in the dark at room temperature. Dissected retinas were preincubated in Ringer's solution (in mM) (130 NaCl, 2.5 KCl, 1 $MgCl_2$, 0.7 $CaCl_2$, 20 $NaHCO_3$, pH 7.2) supplemented with 5 mM glucose prior to the 2-NBDG loading. For the 2-NBDG loading, retinas were first starved for 5 min in low glucose Ringer's solution (0.5 mM glucose) in order to minimize competition with dye transport. Then retinas were loaded with 0.3 mM 2-NBDG in low glucose Ringer's solution for 10 min in the presence or absence of 10 μM FDNB. Excess 2-NBDG was removed by washing retinas twice in regular Ringer's solution for 5 min. Solutions were continuously gassed with 95/5% O_2/CO_2 in order to maintain the pH. For imaging, retinas were flattened on nitrocellulose filter paper and imaged in Ringer's solution with the Olympus FluoView-300 confocal microscope using a 20×, 0.5 NA water immersion objective (Olympus). Image stacks (236 × 236 μm) were recorded through the photoreceptor layer as single optical slices (1 μm). 2-NBDG fluorescence was excited at 488 nm and imaged at 505–550 nm emission. tdTomato was excited at 568 nm and imaged in a separate stack. Because tdTomato specifically labels cone photoreceptors, it was used for orientation and to determine the image stack size. The analysis of NBDG loading was done with NIH ImageJ as follows: First, the cone cell body region where most glucose uptake is expected was identified by the tdTomato signal. Then the fluorescent signal of one optical slice was averaged and summed over five optical slices (encompassing 4 μm). Following this, the 2-NBDG signal was normalized to the tdTomato fluorescent signal in order to adjust for differences in imaging conditions. To determine the relative rates of 2-NBDG uptake, normalized 2-NBDG values of retinas loaded in the presence of FDNB were divided by the normalized 2-NBDG values from control retinas. (*F*) 10 μM FDNB does not affect reduction of all-trans retinal in mouse retinas. All procedures were performed at 4 °C. Eyecups were prepared from enucleated mouse eyes. Tissue samples were homogenized in a Duall glass homogenizer containing 1 mL of 0.1 M MOPS (pH 7.2) and 0.1 M hydroxylamine with 1 mL of ethanol. Following a 15-min incubation at room temperature, the homogenate was transferred to a 16 mm × 100 mm borosilicate tube and extracted twice with 5 mL of hexane. The pooled organic phases were dried under a stream of argon, and the sample was redissolved in 200 μL of hexane. Samples were analyzed with an Agilent 1100 series HPLC equipped with a photodiode array detector on an Agilent Zorbax Rx-Sil 4.6 mm × 250 mm, 5-μm column using a gradient of dioxane in hexane at a flow rate of 2 mL/ min. Spectral data (450–210 nm) were acquired for all eluted peaks. The identity of each eluted peak was established spectrally and by coelution with authentic retinoid standards. Peak areas were determined by comparison to calibration curves established with retinoid standards.

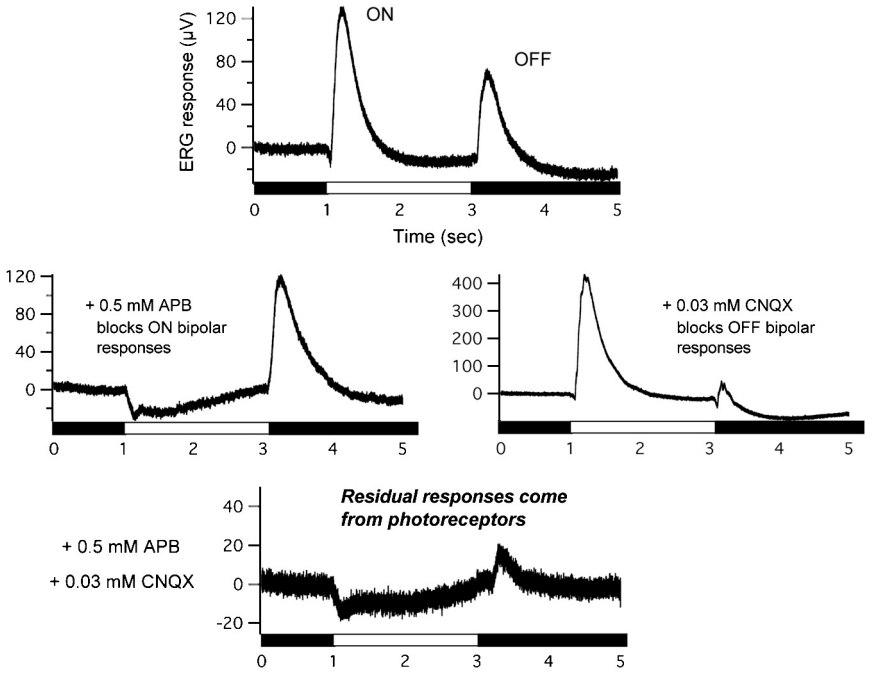

Fig. S8. Analysis of the components of the on and off responses of the larval zebrafish ERG. (*A*) Normal on and off responses to a 2-sec pulse of intense white light (~1 mW/cm^2). (*B*) The mGluR6 agonist 2-amino-4-phosphonobutyrate (APB) blocks the responses of on bipolar cells to the light pulse. (*C*) The ionotropic glutamate receptor antagonist 6-cyano-7-nitroquinoxaline-2,3-dione (CNQX) blocks the responses of off bipolar cells to the light pulse. (*D*) When both APB and CNQX are present, all of the postsynaptic responses are blocked and only the ERG responses originating in the photoreceptors remain.

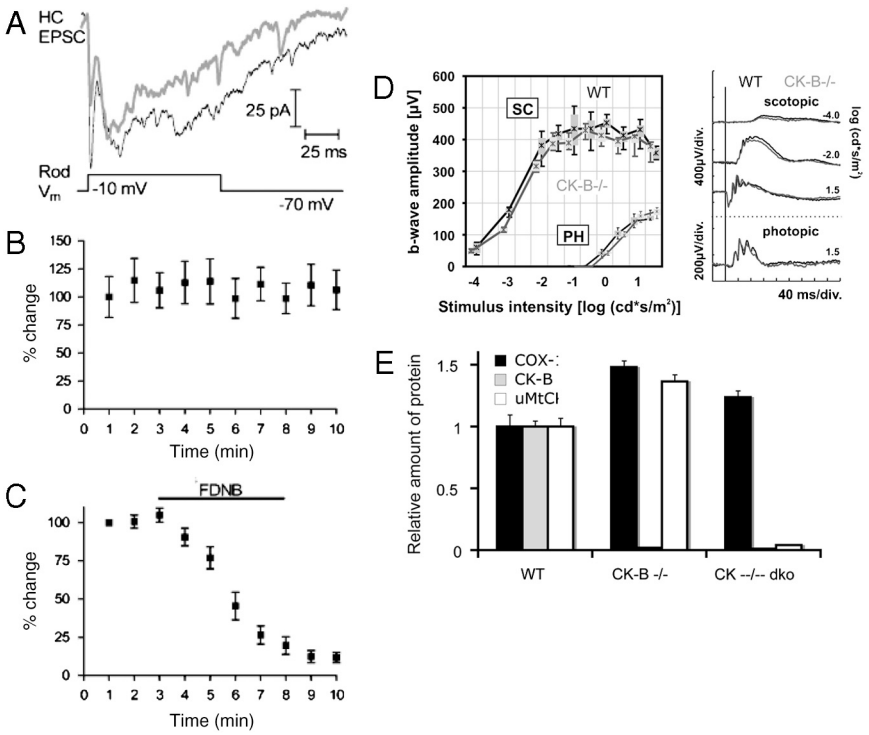

Fig. S9. (*A*) CK activity is essential for synaptic transmission by salamander rods. Example of HC EPSCs in control and after 5 min bath application of FDNB (10 μM) evoked by depolarizing stimulation of a rod. Both fast and slow components of the EPSC were inhibited by FDNB. Slower components of the rod-driven EPSC involve output from gap junctionally coupled neighboring rods as well as contributions from calcium-induced calcium release (9). (*B* and *C*) Effects of FDNB on the amplitude of HC EPSCs evoked by depolarizing steps applied to rods as a function of time ($n = 5$). For the graph, we plotted the amplitude of the fast initial peak of the EPSC. As with cones, FDNB strongly inhibited HC EPSCs evoked by depolarizing stimulation of rods. (*D*) Retinal phenotypes of CK knock-out mice. Comparison of ERGs of WT and CK-B-/- mice. (*Right*) Representative single-flash ERG recordings from dark-adapted (*Top*) and light-adapted (*Bottom*) states of WT (*Black Traces*) and CK-B-/- (*Gray Traces*) mice. (*Left*) Statistical evaluation (box-and-whisker plot) of dark-adapted (scotopic; SC) and light-adapted (photopic; PH) single-flash ERG b-wave amplitudes in WT (*Black*; $n = 3$) and CK-B-/- (*Gray*; $n = 3$) mice. Boxes indicate the 25% and 75% quantile range, whiskers indicate the 5% and 95% quantiles, and the asterisks indicate the median of the data. There was no evidence for differences between WT and CK-B-/- mice. (*E*) Results of quantitative immunoblot analyses of cytochrome oxidase I and uMtCK levels in homogenates of retinas from WT, CK-B-/-, and CK–/– dko mice.